KAVAKA 62(2): 82-88 (2026) DOI: 10.36460/Kavaka/62/2/2026/82-88

Mycogenic Transformation of Iron Rust into Hematite (Fe_2O_3) Quantum Dots: A Comparative Analysis of Antioxidant Activity

Sk Najrul Islam[1], Sadia Parveen[1], Azam Raza[1], Ejaz Ahmad Siddiqui[2], Iqbal Ahmad Siddiqui[2], Mohammad Haris Siddiqui[2], and Absar Ahmad[1*]

1Interdisciplinary Nanotechnolcogy Centre (INC), Z. H. College of Engineering and Technology, Aligarh Muslim University, AMU, Aligarh, UP-202002, India.

[2]Department of Biosciences, Integral University, Lucknow, UP 226026, India.

**Corresponding Author Email: aahmad786in@gmail.com*

(Submitted on 5 March, 2026; Accepted on 22 May, 2026)

ABSTRACT

Mycogenic transformation approaches are well established as sustainable and environmentally friendly strategies for the conversion of waste into valuable materials. Herein, micron-sized rust particles were biotransformed into highly stable and water-dispersible hematite quantum dots (α-Fe_2O_3 QDs) using the endophytic fungus *Fusarium oxysporum*. Different characterization techniques such as Transmission Electron Microscopy (TEM), Fourier Transformed Infrared Spectroscopy (FTIR), and Photoluminescence (PL) were performed to characterize α-Fe_2O_3 QDs. Furthermore, we evaluated comparative antioxidant activity using DPPH 2,2-diphenyl-picrylhydrazyl) scavenging for both rust particles and α-Fe_2O_3 QDs. The results showed a scavenging efficiency of 5.82% for rust particles and 97.5% for α-Fe_2O_3 QDs, demonstrating that QDs exhibit superior antioxidant efficacy compared to rust particles.

Keywords: *Fusarium oxysporum*, Endophytic, Biotransformation, α-Fe_2O_3 QDs, Antioxidant activity

INTRODUCTION

Iron has been utilized by humans for thousands of years and has played a crucial role in shaping human civilizations and contributed to their progress and development (Paula, 1960; Weeks, 1968). Iron-based materials play a vital role in daily life, including infrastructure, transportation, household tools and appliances, industrial machinery, medical and healthcare applications, etc. (Greenwood & Earnshaw, 2012; Yee & Tolman, 2015). Despite its usefulness, when iron is exposed to moist air for a considerable period, it undergoes oxidation, resulting in the formation of a reddish-brown flaky substance on its surface (Gräfen *et al*., 2000). This soft and porous material commonly referred to as rust, can degrade the structural integrity and aesthetics of iron, rendering it less effective; the formed rust serves little practical purpose. Against this background, Iron oxide nanoparticles hold a unique place in the realms of nanoscience and nanotechnology due to their remarkable stability, biocompatibility, and magnetic properties. Different types of iron oxide compounds (FeO, Fe_2O_3, and Fe_3O_4) with different structural phases (α-Fe_2O_3, β-Fe_2O_3, γ-Fe_2O_3, and ε-Fe_2O_3) find wide-ranging applications in the field of medicine, technology and fundamental research (Kumar *et al*., 2014; Maji *et al.,* 2012; Mohapatra and Anand, 2011; Upadhyay *et al*., 2016). Hematite (α-Fe_2O_3), a form of iron oxide is chemically stable and possesses valuable n-type semiconductor characteristics with band-gap in the range of 2.1–2.2 eV, rendering it as excellent material (Atyam *et al.*, 2015). Its wide availability, affordability, minimal toxicity, and tunable magnetic and optical properties make α-Fe_2O_3 nanoparticle, a subject of significant interest in diverse domains. These include catalysis, sensors, solar cells, water splitting, and lithium-ion batteries etc (Atyam *et al*., 2015; Jing and Wu, 2005; Niu *et al*., 2013; Sun *et al*., 2010; Wheeler *et al*., 2012; Zhang and Li, 2008). The properties of α-Fe_2O_3 nanoparticles can undergo significant enhancement when their dimensions are less than 10 nm, a size range often referred to as quantum dots (QDs), due to the increased surface area (Wang *et al*., 2016). To date, various methods have been reported for producing α-Fe_2O_3 nanoparticles with diverse sizes and shapes. However, almost all of the α- Fe_2O_3

nanoparticles are synthesized either through conventional solution-based methods or by the transformation of as-synthesized ferric oxyhydroxide nanoparticles via calcination (Liu *et al*., 2007; Piao *et al*., 2008; Tadic *et al*., 2014; Yan *et al*., 2014).

At present, rust is valued for being a stable, affordable, and environmentally benign precursor in physicochemical production of hematite nanoparticles that have been effectively utilized as catalysts for organic synthesis, photocatalysts for dye degradation, agents for hydrogen evolution, and redox-active electrodes in batteries (Babar et al., 2018; Gurav *et al*., 2020; Mikucki *et al*., 2009; Salunkhe *et al*., 2021), much like turning trash into treasure. Nonetheless, to the best of our knowledge there have been no reports so far, of utilizing rust Micron-sized particles as an initial material for the biotransformation into Fe_2O_3 QDs. In this study, we explored a fungal-mediated approach for the sustainable production of Fe_2O_3 QDs using micron-sized rust particles as the starting material, unlike traditional methods using soluble precursors. Interestingly, our research revealed that fungus effectively biotransformed such large-sized rust particles into QDs with distinct phases and shapes, differing from the parent materials. In this study, we have also conducted comparative evaluations of antioxidant activity using DPPH scavenging for both rust particles and Fe_2O_3 QDs.

MATERIALS AND METHODS

Materials

Iron wire was acquired from the local shop of Aligarh, Uttar Pradesh, India. D-glucose was obtained from Qualigens, while peptone, yeast, and malt extract were procured from Hi-media for the preparation of the fungal media. 2,2-diphenyl-1-picrylhydrazyl (DPPH) was purchased from Alfa Aesar and all other chemicals utilized in the analysis were used in their original form as received from commercial suppliers.

Fungal growth, formation and biotransformation of rust

The fungus, *Fusarium oxysporum*, was cultured following the same procedures outlined in previous studies (Islam *et al*., 2021). After incubation, the fungal mycelia were carefully harvested and subjected to meticulous washing under sterile conditions. The obtained fungal biomass (30 g wet weight) was subsequently employed for the biotransformation of rust.

On the contrasting side, approximately 50 cm of iron wire was subdivided into smaller fragments and thoroughly cleaned with sterilized water (**Figure 1a**). These iron fragments were subsequently exposed to the formation of rust by being immersed in 100 ml of water within 250 ml Erlenmeyer flasks for a duration of 10–15 days at room temperature. Subsequent to this period, the water's colour chage to brown validated the rust formation. The resulting brown solution was then subjected to filtration and lyophilization to facilitate further experimental procedures and characterization (**Figure 1b and 1c**).

To carry out the biotransformation of rust using *Fusarium oxysporum*, the harvested fungal biomass (30 g wet weight) was reconstituted in 100 ml of autoclaved double-distilled water containing 100 mg of lyophilized rust powder in a 500 ml flask under consistent agitation conditions (250 rpm) at 25°C temperature. After 96 hours of continuous shaking (250rpm) at a temperature of 25°C, the solution's colour changed to reddish-orange, serving as a primary indication of iron oxide quantum dot formation. The mycelial mass was subsequently separated using Whatman filter paper, and the resulting filtrate was lyophilized into powder, facilitating more convenient handling and subsequent characterization processes.

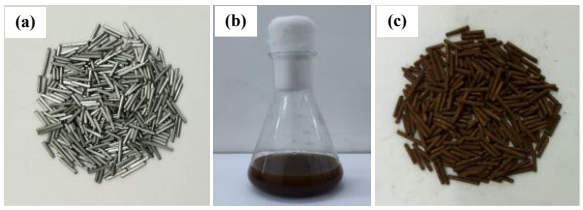


Figure 1: (a) Iron wires, (b) Rusted iron wires fragments in water (after 10-15 days) and (c) Rusted iron wires.

Characterization techniques

Transmission Electron Microscopy (TEM) measurements were carried out to reveal the morphology of the bio-transformed rust particles using a JEOL JEM 2100F instrument at an accelerating voltage of 200 kV. The Fourier Transform Infrared Spectrometer (FTIR) spectrum was employed to identify the presence of different chemical bonds and the vibrational frequencies of

biomolecules coated on α-Fe_2O_3 QDs. This spectrum was acquired using a Perkin Elmer Fourier Transform Infrared Spectrometer, covering a wavenumber range of 400 to 4000 cm^{-1}. To investigate the structural and crystallographic characteristics of the α-Fe_2O_3 QDs and rust particles, X-ray diffraction (XRD) analysis was conducted. This analysis utilized a Rigaku X-ray diffractometer equipped with high-intensity Cu-Kα radiation (λ = 1.5406 Å) in 2θ range of 20° to 80° with a scanning rate set at 5°/min. Optical analysis was carried out utilizing a Fluorescence spectrometer (Perkin Elmer LS-55) at different excitation wavelengths.

Antioxidant activity

The antioxidant activity of both α-Fe_2O_3 QDs and micron-sized rust particles was assessed through the reduction of the radical 2,2-Diphenyl-1-picrylhydrazyl (DPPH). Initially, a standard methanolic solution of DPPH of 0.01 mM was prepared, along with the different concentrations (ranging from 62.5 to 1000 µg/ml) of aqueous rust particles and α-Fe_2O_3 QDs were prepared separately. Subsequently, 2 ml of DPPH solution was mixed with 1 ml of α-Fe_2O_3 QDs suspension at different concentrations and left to incubate in the dark for 10 min at room temperature. Following this incubation period, the absorbance of all samples was measured, with methanolic DPPH without QDs serving as the control and methanol acting as the blank. The percentage of DPPH scavenging was determined using the following formula:

$$\%\, Scavenging = \frac{A_o - A_s}{A_o} * 100$$

where "A_o" and "A_S" represent the absorbance of the control and sample, respectively. For comparative study, we also conducted the antioxidant activity assessment of rust particles using the same procedure as previously employed for α-Fe_2O_3 QDs.

RESULTS AND DISCUSSION

Rust particle and Hematite QDs characterization

The TEM micrograph (Figure 2) was captured at a magnification of 100,000X to determine the shape and size of both rust particles and biotransformed α-Fe_2O_3 QDs. From Figure 2(a) it is very clear that the rust particles are of micron size and irregularly shaped. Figure 2(b) and 2(c) represent the TEM images of the biotransformed α-Fe_2O_3 QDs obtained after reacting rust particles with fungus Fusarium oxysporum for 96 h. The biotransformed α- Fe_2O_3 QDs are nearly spherical-shaped and are of size less than 10 nm. As observed in the TEM images, the micron-sized rust particles undergo fragmentation, transforming into smaller spherical particles as a result of their interaction with fungal biomass. It is evident that this process offers substantial advances, as it effectively transforms what was once considered waste into a valuable resource.

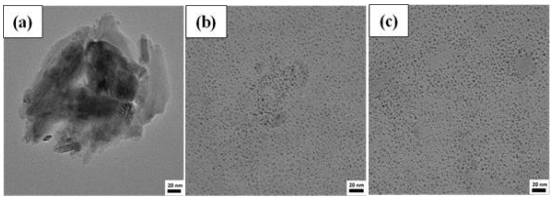


Figure 2: TEM micrograph (a) rust particles and (b, c) biotransformed Hematite quantum dots.

Figure 3(a) showed the comparison between X-ray diffraction patterns of rust particles and biotransformed hematite quatum dots. The diffractogram of rust particles which appeared at 35.04° and 62.16° can be assigned for crystallographic planes (211) and (002) of akaganeite phases of ferric oxyhydroxide (β-FeOOH) (Rajakaruna *et al*., 2021). This β-FeOOH micron sized particles after reacting with fungus *Fusarium oxysporum* for 96 h at 25°C biotransformed into hematite phase of iron oxide (α-Fe_2O_3). The specific crystallographic phase of α-Fe_2O_3 QDs was confirmed by their characteristic diffraction peaks that emerged at 28.2°, 40.44°, 50.04°, 66.32° and 73.64° corresponding to Miller indices (012), (113), (024), (300), and (220) respectively (Bilesky-jose *et al*., 2021; Rajakaruna *et al*., 2021). The comparative FTIR study (Figure 3b) of the α- Fe_2O_3 QDs and rust particles provided insights into the vibration bonds and functional groups of biomolecules responsible for biotransformation and stability. The FTIR spectrum of QDs reveals peaks at 1560 cm^{-1} and 1405 cm^{-1}, corresponding to amide (I and II) bond vibrations, indicate that QDs are capped by protein molecules, rendering them water-dispersible and stable (Islam et al., 2022; Parveen *et al*., 2022). The biotransformed α-Fe_2O_3 QDs also exhibited stretching and bending of Fe-O bond vibrations in the range of 500-600 cm^{-1} and a Fe-OH vibration band at wavenumber 674 cm^{-1} (Rajakaruna *et al*., 2021; Sunny *et al*., 2018). These vibrational bands

were absent in the FTIR spectrum of rust particle. In contrast, the rust FTIR graph showed intense characteristic peaks at 888 cm^{-1} indicating the presence of the characteristic bending vibration of Fe–O–H in β-FeOOH which is absent in QDs, revealing the biotransformation of rust particles (Iiu *et al*., 2016).

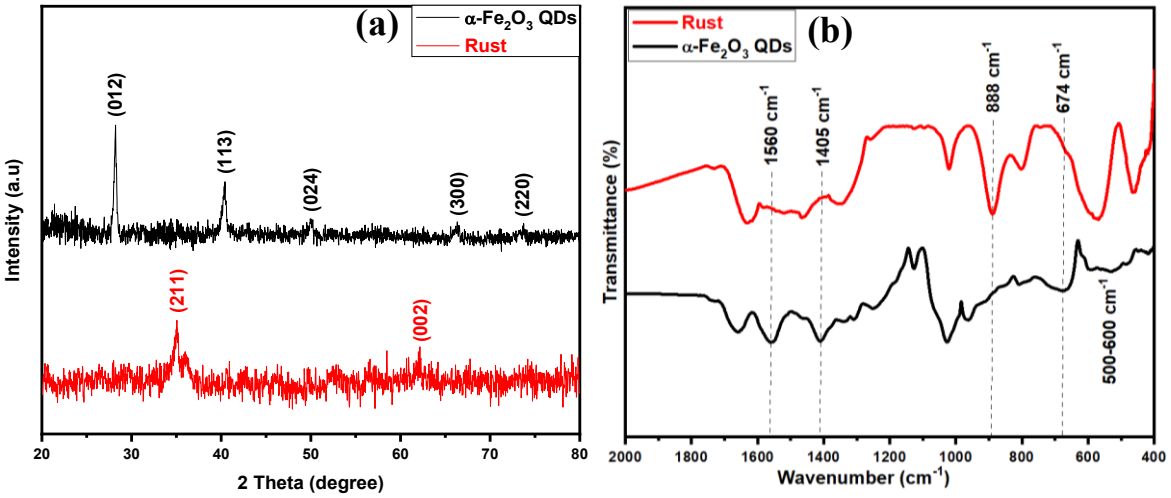


Figure 3: (a) X-ray powder diffractograms and (b) FTIR spectra of α-Fe_2O_3 QDs and rust particles (β-FeOOH).

To investigate the photoluminescence properties of the micron-sized rust particles and biotransformed α-Fe_2O_3 QDs, fluorescence measurements were conducted by exciting aliquots of their solutions at 340nm. The findings indicate that α-Fe_2O_3 QDs exhibit a fluorescence emission peak at approximately 412 nm, whereas no emission peak is observed in rust particles as depicted in Figure 4(a). Moreover, as illustrated in Figure 4(b), we observed a shift in fluorescence emission bands from 345 nm, 375 nm, 373 nm, and 386 nm when the excitation wavelength increased from 320 nm, 330 nm, 330 nm, to 350 nm for QDs. This shift could be attributed to the heterogeneous size distribution of α-Fe_2O_3 QDs. The insert of Figure 4(b) shows QDs in (i) day light and when irradiated at (ii) higher wavelength and (iii) lower wavelength.

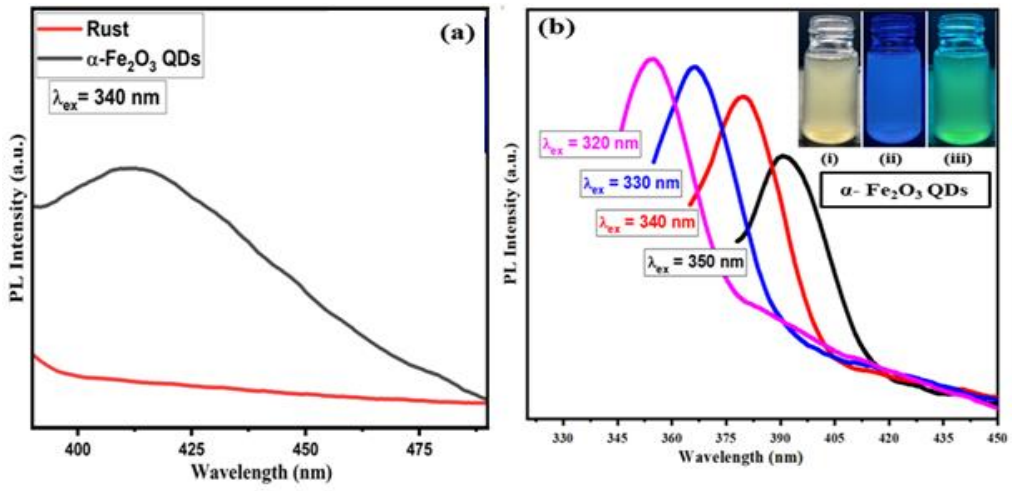


Figure 4: Photoluminescence spectrum of the (a) rust particles and biotransformed α-Fe_2O_3 QDs and (b) Fluorescence emission at different excited wavelength.

Comparative analysis of antioxidant activity

In this study, we investigated the DPPH scavenging efficacy of rust particles and α-Fe_2O_3 QDs by analyzing UV-vis absorbance spectra at 517 nm. For this, different concentrations of rust particles (R1=62.5µg/ml, R2=125µg/ml, R3=250µg/ml,

R4=500µg/ml, R5=1000µg/ml) and α-Fe_2O_3 QDs (N1=62.5µg/ml, N2=125µg/ml, N3=250µg/ml, N4=500µg/ml, N5=1000µg/ml) were used in the study. Rust particles showed no decrease in DPPH absorbance with increasing concentrations (Figure 5a) while the absorbance of DPPH decreased with increasing concentrations of QDs (**Figure 5b**). Biotransformed α-Fe_2O_3 QDs displayed superior antioxidant potency compared to micron-sized rust particles, with 97.5% and 5.82%, respectively, scavenging efficiency observed within 10 minutes at a concentration of 1000 µg/ml (**Figure 5c**).

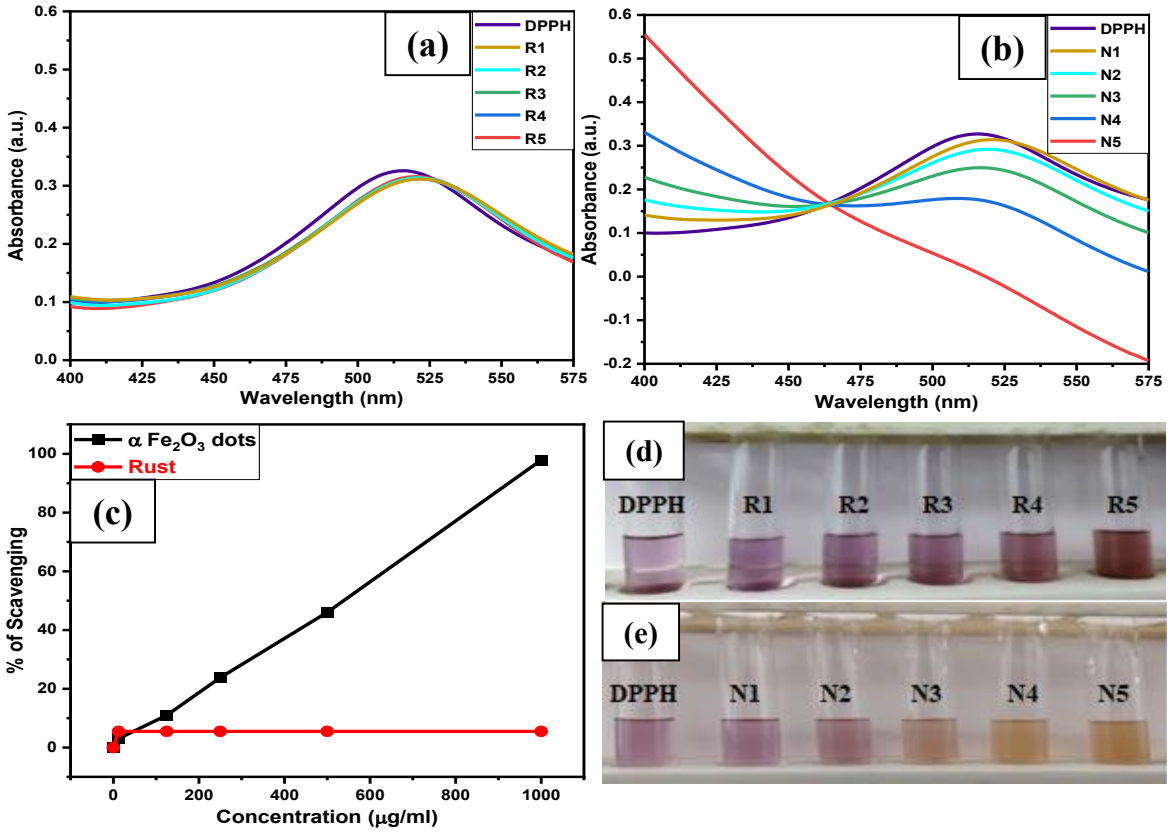


Figure 5: The UV-Vis spectra of DPPH with increasing concentration of (a) rust particles and (b) α-Fe_2O_3 QDs, (c) Concentration-dependent scavenging efficacy, and Colour of DPPH after 10 min at different concentration of (d) rust and (e) α-Fe_2O_3 QDs.

CONCLUSIONS

In this study, we have demonstrated the potential of *Fusarium oxysporum* in the biotransformation of waste iron rust particles into biomedically and technologically valuable α-Fe_2O_3 QDs. These α-Fe_2O_3 QDs exhibit excitation dependent photoemission and superior antioxidant potency with a 97.5% scavenging efficiency in DPPH analysis, surpassing rust particles, which showed only 5.82% scavenging efficiency. In summary, this mycogenic transformation approach can be broadly extended to convert diverse inorganic wastes into high-value materials, offering a versatile and dynamic platform for advancing next-generation applications such as drug delivery systems, cosmetics, antimicrobial gels and coatings, therapeutics, and theranostics.

ACKNOWLEDGMENTS

We acknowledge the Department of Biotechnology (DBT), Government of India, for setting up a Centre of Excellence (COE, BT/PR1-3584/COE/34/29/2015) at Interdisciplinary Nanotechnology Centre (INC), Aligarh Muslim University, AMU, Aligarh, UP-202002, India. SNI sincerely acknowledge the financial support provided by the Council of Scientific & Industrial Research (CSIR), India, through the award of a Research Associateship (RA) (File No. [09/0112(23407)/2025-EMR-I]).

Conflict of Interest

The authors have declared no conflict of interest.

REFERENCES

Atyam, K. K., Ghosh, A., Mukherjee, K., *et al.* 2015. Hematite iron oxide nano-particles: facile synthesis and their chemi-resistive response towards hydrogen. *Materials Research Express*, **2(5)**, 55901.

Babar, S., Gavade, N., Shinde, H., *et al.* 2018. Evolution of Waste Iron Rust into Magnetically Separable g-C3N4 –Fe_2O_3 Photocatalyst: An Efficient and Economical Waste Management Approach. *ACS Applied Nano Materials*, **1(9),** 4682–4694.

Bilesky-jose, N., Maruyama, C., Germano-costa, T., et al. 2021. Biogenic α - Fe_2O_3 Nanoparticles Enhance the Biological Activity of Trichoderma against the Plant Pathogen *Sclerotinia sclerotiorum. Sustaining Life on Planet Earth: Metalloenzymes Mastering Dioxygen and Other Chewy Gases,* pp 131–204.

Gräfen, H., Horn, E.-M., Schlecker, H., *et al*. 2000. Corrosion. *Ullmann's Encyclopedia of Industrial Chemistry*. Wiley-VCH Verlag GmbH & Co. KGaA.

Greenwood, N. N., and Earnshaw, A. 2012. *Chemistry of the Elements*. Elsevier.

Gurav, R., Surve, S. K., Babar, S., *et al*. 2020. Rust-derived Fe_2O_3 nanoparticles as a green catalyst for the one-pot synthesis of hydrazinyl thiazole derivatives. *Organic & Biomolecular Chemistry*, **18(24)**, 4575–4582.

Iiu, Y., Lv, J., Jin, W., *et al*. 2016. Defluoridation by rice spike-like akaganeite anchored graphene oxide. *RSC Advances*, **6(14)**, 11240–11249.

Islam, S. N., Naqvi, S. M. A., Parveen, S., *et al*. 2021. Application of mycogenic silver/silver oxide nanoparticles in electrochemical glucose sensing; alongside their catalytic and antimicrobial activity. *3 Biotech*, **11(7)**, 1–11.

Islam, S. N., Raza, A., Naqvi, S. M. A., *et al*. 2022. Unveiling the antisporulant activity of mycosynthesized gold-selenide nanoparticles against black fungus *Aspergillus niger*. *Surfaces and Interfaces*, **29**, 101769.

Jing, Z. H., Wu, S. H. 2005. Preparation and magnetic properties of spherical α-$F_{e2}O_3$ nanoparticles via a non-aqueous medium. *Materials Chemistry and Physics*, **92(2)**, 600–603.

Kumar, B., Smita, K., Cumbal, L., *et al*. 2014. Biogenic synthesis of iron oxide nanoparticles for 2-arylbenzimidazole fabrication. *Journal of Saudi Chemical Society*, **18(4)**, 364–369.

Liu, X., Qiu, G., Yan, A., *et al*. 2007. Hydrothermal synthesis and characterization of α-FeOOH and α-Fe_2O_3 uniform nanocrystallines. *Journal of Alloys and Compounds*, **433**, 216–220.

Maji, S. K., Mukherjee, N., Mondal, A., 2012. Synthesis, characterization and photocatalytic activity of α-Fe_2O_3 nanoparticles. *Polyhedron*, **33(1)**, 145–149.

Mikucki, J. A., Pearson, A., Johnston, D. T., *et al*. 2009. A Contemporary Microbially Maintained Subglacial Ferrous "Ocean." *Science*, **324(5925)**, 397–400.

Mohapatra, M., and Anand, S. 2011. Synthesis and applications of nano-structured iron oxides/hydroxides – a review. *International Journal of Engineering, Science and Technology*, **2(8)**.

Niu, H., Zhang, S., Ma, *et al*. 2013. Dye-sensitized solar cells based on flower-shaped α-Fe_2O_3 as a photoanode and reduced graphene oxide–polyaniline composite as a counter electrode. *RSC Advances*, **3(38)**, 17228–17235.

Parveen, S., Najrul Islam, S., *et al*. 2022. Mycological synthesis of Ruthenium oxide quantum dots and their application in the colorimetric detection of H_2O_2. *Advanced Powder Technology*, **33(12)**, 103861.

Paula, M. 1960. *The Forging of Israel Iron Technology, Symbolism and Tradition in Ancient Society*. Bloomsbury Publishing.

Piao, Y., Kim, J., Na, H. Bin, *et al*. 2008. Wrap-bake-peel process for nanostructural transformation from B-FeOOH nanorods to biocompatible iron oxide nanocapsules. *Nature Materials*, **7(3)**, 242–247.

Rajakaruna, T. P. B., Udawatte, C. P., Chandrajith, R., *et al*. 2021. Formulation of Iron Oxide and Oxy-hydroxide Nanoparticles from Ilmenite

Sand through a Low-Temperature Process. ACS Omega, **6**, 17824–17830.

Salunkhe, T. T., Varma, R. S., Kadam, A. N., *et al*. 2021. Scraps to superior anodes for Li-ion batteries: Sustainable and scalable upgrading of waste rust. *Journal of Hazardous Materials*, **410**, 124571.

Sun, B., Horvat, J., Kim, H. S., *et al*. 2010. Synthesis of Mesoporous α-Fe_2O_3 Nanostructures for Highly Sensitive Gas Sensors and High-Capacity Anode Materials in Lithium-Ion Batteries. *The Journal of Physical Chemistry C*, **114(44),** 18753–18761.

Sunny, A., Prasad, N., Subbaiyan, D., *et al*. 2018. Optical, vibrational and fiber optic gas-sensing properties of hematite microparticles. *Applied Physics A: Materials Science and Processing*, **124(10)**, 1–8.

Tadic, M., Panjan, M., Damnjanovic, V., *et al*. 2014. Magnetic properties of hematite (α-Fe_2O_3) nanoparticles prepared by hydrothermal synthesis method. *Applied Surface Science*, **320**, 183–187.

Upadhyay, S., Parekh, K., and Pandey, B. 2016. Influence of crystallite size on the magnetic properties of Fe_3O_4 nanoparticles. *Journal of Alloys and Compounds*, **678**, 478–485.

.

Wang, J., Zhang, N., Su, J., and Guo, L. 2016. α-Fe*2*O*3* quantum dots: Low-cost synthesis and photocatalytic oxygen evolution capabilities. *RSC Advances*, **6(47)**, 41060–41066.

Weeks, E. M. 1968. *Discovery of the elements*. Journal of chemical education.

Wheeler, D. A., Wang, G., Ling, Y., Li, Y., & Zhang, J. Z. 2012. Nanostructured hematite: synthesis, characterization, charge carrier dynamics, and photoelectrochemical properties. *Energy & Environmental Science*, **5(5)**, 6682–6702.

Yan, H., Su, X., Yang, C., Wang, J., and Niu, C. 2014. Improved photocatalytic and gas sensing properties of α- Fe_2O_3 nanoparticles derived from β-FeOOH nanospindles. *Ceramics International*, **40(1 PART B)**, 1729–1733.

Yee, G. M., & Tolman, W. B. 2015. Transition Metal Complexes and the Activation of Dioxygen. *Sustaining Life on Planet Earth: Metalloenzymes Mastering Dioxygen and Other Chewy Gases* (pp. 131–204).

Zhang, X., and Li, Q. 2008. Microwave assisted hydrothermal synthesis and magnetic property of hematite nanorods. *Materials Letters*, **62(6–7)**, 988–990.

.